Random Tropospheric Angle Errors in Microwave Observations of the Early Bird Satellite

By J. H. W. UNGER

(Manuscript received June 16, 1966)

A simplified analytical model of tropospheric random variations in angle measurements is described. This model is used to predict the minimum and maximum power density spectra between which the tropospheric random angle errors of observations on the Early Bird satellite are expected to lie.

The apparent angular position of the Early Bird satellite was then measured at microwave frequencies with the large horn-reflector antenna at the AT&T station near Andover, Maine. Random variations in the azimuth and elevation angles have been observed and recorded. The analysis of these records results in a description of the observed random angle variations by their power density spectra.

A comparison of the predicted power density spectra from the model with the observed spectra is made. It is concluded that the observed random angle variations are indeed caused by random tropospheric refraction.

The feasibility of acquiring data on atmospheric propagation effects, particularly tropospheric angle errors, with the aid of geo-stationary satellites is therefore also demonstrated.

I. INTRODUCTION

1.1 *Objective of this Paper*

The performance of earth-based radar and optical systems is ultimately limited by temporal and spatial random variations in the refractive index of the tropospheric propagation medium. It is the objective of this paper to present a method for predicting random tropospheric angle errors in such systems, and to compare a prediction with microwave observations made on the Early Bird satellite.

1.2 *Problem Approach*

The scintillation or twinkling of the stars which is experienced in observations through the earth's troposphere is a familiar effect of the random variations in the refractive index of this propagation medium. Astronomers have known for a long time that the troposphere actually causes variations in at least four characteristics of the received star light, namely: (*i*) the intensity, (*ii*) the spectral distribution of the intensity, (*iii*) the shape of the telescopic diffraction image, and (*iv*) the apparent angular position of the star. Scientific studies[1,2] of these effects seem to concentrate mainly on the intensity scintillations. The random variations in the other characteristics, especially in the apparent angular positions of stars, are treated in much less detail.

However, in those radar and optical systems which are used to measure the position (and its time derivatives) of both distant and near objects (such as aerospace vehicles) the random tropospheric angle variations assume great importance. For the analysis and synthesis of these systems, it is valuable to accumulate the knowledge on the random tropospheric errors in form of a sufficiently general model.

Such an analytical model of tropospheric random errors in the position measurements and their time derivatives in radar and optical systems has been developed. Among other capabilities this model also permits the prediction of the random tropospheric angle variations for specified sets of tracking situations and system parameters. The prediction is made in terms of minimum and maximum power density spectra (PDS) between which the observed spectra are expected to lie.

The choice of PDS for the characterization of the random errors is necessary because the relation between errors at two points in this system is usually a function of the error frequency (f). The resulting PDS further permit (*i*) subsequent studies of the effects of frequency dependent data processing operations (smoothing, calculation of derivatives, prediction, etc.). (*ii*) detailed comparison with errors from other sources, and (*iii*) application of the optimization methods described by H. W. Bode, C. E. Shannon, and S. Darlington.[3] Values for the more familiar variance (σ^2) or standard deviation (σ) of these random errors at the output of these processes may then be obtained with a straightforward integration of the output PDS (see Section 1.4 below).

Within the model, the predicted PDS of the random tropospheric angle errors are analytically calculated by operating with certain model functions on a model power density spectrum which is given in the range coordinate. This range model PDS represents the pooled data on tropospheric random refraction. It is based upon observations of random

variations in the tropospheric refractive index, and in range and phase measurements mainly made at the National Bureau of Standards.[4,5,6,7]

The successful launch of the Communications Satellite Corporation's Early Bird Satellite on April 6, 1965, and its subsequent stabilization in an almost perfect geo-stationary orbit, provided an opportunity to test the model. For this purpose, azimuth and elevation angle measurements on the microwave beacon of the Early Bird satellite were made with the large horn-reflector antenna at the American Telephone and Telegraph (AT &T) Station near Andover, Maine. Most of this ground equipment was previously described in detail.[9,10,11,12,13,14,15] A brief description of the Early Bird satellite may be found in Ref. 16.

The resulting angle error measurements are particularly valuable for comparison with the theoretical model since they are obtained under two unique conditions provided by a geo-stationary satellite as a target. First, the propagation path goes through the entire atmosphere so that the observed angle errors include possible effects of high altitude turbulence, which are impossible to obtain with Earth based targets. Second, the angular tracking rates are negligible relative to the effective wind in the troposphere with which the refractive index anomalies pass through the propagation path.

Thus, the analysis of the angle error measurements and the prediction of the expected random angle errors for the geo-stationary satellite are considerably simplified compared to the analysis and prediction for the more frequent aerospace targets (aircraft, missiles, low satellites) which have large apparent angular velocities and motion disturbed by forces unknown in the necessary detail. The effects of temporal random variations of the refractive index in the Earth's atmosphere on the angle measurements, integrated along the line-of-sight between a ground antenna and a geo-stationary satellite should be observable in an almost pure form.

1.3 *Scope of this Paper*

In this paper, a simplified version of the model of random tropospheric errors is first described, which permits the calculation of the predicted minimum and maximum PDS of the tropospheric angle errors for tracking tasks involving one almost stationary point target and a single observer (single-site radar).

Next, the presented model is used to calculate the numerical values of the predicted PDS of random tropospheric angle errors for the specific tracking situation of the Early Bird observations.

The methods and specific circumstances of data acquisition for one

twenty minute period of observations of the Early Bird satellite from the AT &T ground station near Andover, Maine are then described. Another section is concerned with data processing and analysis; it includes the time series of observed azimuth and elevation angles, the calculations of their power density spectra and confidence limits, and estimates of the manual chart reading error and of the effects of thermal receiver noise.

Finally, a comparison is made between the PDS of random tropospheric angle errors predicted with the model and the PDS of the observed random angle variations.

1.4 *Scaling of Power Density Spectra*

In this paper, the random variations of the observed azimuth and elevation angles will be described by their power density spectra (PDS). The numerical computation of the PDS from the time series of data is made by the indirect method described by Blackman and Tukey.[17] However, the scaling of the PDS in this paper deviates from that of Blackman and Tukey by defining the variance σ^2 of the random error as

$$\sigma^2 = \int_0^\infty P\{f\}df. \tag{1}$$

Thus, the PDS $P\{f\}$ is valid only for positive frequencies, $f \geqq 0$. The power spectral density is

$$P\{f\} = \frac{d(\sigma^2)}{df} \tag{2}$$

of the variance contribution $d(\sigma^2)$ to the random error, per unit frequency bandwidth, df, at the frequency, f.

II. PREDICTION OF RANDOM TROPOSPHERIC ANGLE ERRORS

2.1 *Model Concept*

The analytical model of random tropospheric errors in radar and optical systems which has been developed permits the calculation of the power density spectra, and variances of range, phase, range difference, and angle errors, and their time derivatives from a basic pool of model data with the aid of certain model functions. This general model accommodates many different sets of system parameters, and is flexible enough to allow modification for its continuing improvement based upon the analysis of additional data.

During the development of the model the usual lack of sufficient data, and the non-stationarity of the tropospheric refractivity field soon made

themselves felt. It was realized therefore, that only an approximate model of the real troposphere could readily be constructed, which necessarily would yield approximate predictions. However, it was found that this approximate model was good enough to allow the useful prediction of tropospheric errors in several interesting cases of tracking system analysis and synthesis.

In the following part of this paper a simplified version of the general model of random tropospheric errors is described, which is limited to the prediction of the power density spectra of the random tropospheric errors in the *angle* measurements made by a *single-site* radar (or radio tracker) on an (almost) *stationary target.*

The particular coordinate of radar measurements selected for the collective description of the pool of basic model data is the slant-range coordinate. In this approach, all available observations of random tropospheric errors are first normalized to certain model conditions, and transformed into the slant-range coordinate. An analytical power density spectrum (PDS) at the lower limit of these normalized and transformed observations is then defined as the model PDS in range, $P_m\{f\}$, where f is the (error-) frequency.

The derivation of the PDS for the random tropospheric angle errors, and for other than the model conditions, is then achieved by processing the range model PDS, $P_m\{f\}$, with certain power gain functions, called the model functions. These model functions depend on such parameters of the tracking situation as the antenna diameter, slant-range and elevation angle of the target, weather, and wind.

It may be noted particularly, that in this simplified version of the model it is not necessary to do any explicit processing in the space domain. Based upon the assumption of an isotropic, and frozen turbulence field of refractive index anomalies in the troposphere, all processing is confined to the frequency $\{f\}$-domain.

The entire model also can be used in an inversion of the computational flow to yield, from new observations, additional information on the basic range model PDS, $P_m\{f\}$, and on the model functions.

2.2 *Assumptions and Limitations*

The simplified analytical model of tropospheric random errors in radar and optical systems is subject to a number of assumptions and limitations:

(*i*) The model is intended to yield tropospheric errors in tracking tasks where one point target is directly observed within the local horizon along a line-of-sight (LOS) by a single observer.

(*ii*) It is assumed that the random errors are small, thus the model functions are linear in the sense of being independent of the magnitude of the errors.

This assumption is justified by the finding that the random errors in the observed quantities (range, angles) have relative magnitudes of only one part in 10^5, or so.

(*iii*) It is assumed that the random errors are stationary during the calculation, or observation of one PDS. The spatial and temporal non-stationarities of the random tropospheric errors are only considered by the introduction of the "global" weather functions. Local anomalies, as well as diurnal and seasonal variations of the tropospheric random errors thus are not separated here. It is believed that more detailed knowledge in this respect is better obtained by direct measurements under the particular local circumstances of actual tracking situations.

(*iv*) It is assumed that the random errors due to the tropospheric anomalies can be treated as if they were caused by the motion of a locally isotropic field of "frozen" turbulence through the line-of-sight with an effective wind speed (**u**) normal to the LOS.

(*v*) The wavelength (λ) of the transmitted electromagnetic waves is assumed to be small, say $\lambda \leqq 10$ [cm], in order to avoid basic theoretical difficulties which are manageable only if $\lambda \ll l$, where l is the characteristic length of the tropospheric anomalies.[1,2] This assumption is also important in order to avoid the effects of random propagation through the ionosphere.

(*vi*) The size of the antenna system is small with respect to the diameter of the earth (flat earth assumption).

(*vii*) The size of the antenna system is small enough to avoid the lack of correlation between the refractivity anomalies at large distances on the surface of the earth.

2.3 *Model Functions*

2.3.1 *Model Power Density Spectrum in Range, $P_m\{f\}$*

The conditions to which the available data[4,5,6,7] on random tropospheric range, phase, and refractive index variations are normalized are:

(*i*) effective tropospheric path length = $L_m = 15$ [km];

(*ii*) effective wind speed normal to LOS = $u_m = 1$ [m/sec];

(*iii*) surface refractivity = $N_m = 10^6\ (n_m - 1) = 313$, this value is the U.S. average,[8] and n_m is the equivalent refractive index;

(*iv*) known effects of variations of the surface refractivity are not corrected during data acquisition.

After transformation to the selected range coordinate the model power density spectrum, $P_m\{f\}$, is then derived as an analytical approximation to the *lower* limit of all observations.

The derived model PDS in range consists of five branches, which are linear in a log (power density) versus log (frequency) plot, namely:

$$P_m\{f\} = \begin{cases} 9.6 \times 10^{+19} f^{+2} \text{ [m}^2\text{/Hz]} \\ \qquad \text{for} \quad 0 \leqq f \leqq 2.5 \times 10^{-8} \text{ [Hz]} \\ 1.5 \times 10^{-3} f^{-1} \text{ [m}^2\text{/Hz]} \\ \qquad \text{for} \quad 2.5 \times 10^{-8} \leqq f \leqq 1.0 \times 10^{-5} \text{ [Hz]} \\ 4.7 \times 10^{-11} f^{-2.5} \text{ [m}^2\text{/Hz]} \\ \qquad \text{for} \quad 1.0 \times 10^{-5} \leqq f \leqq 1.0 \times 10^{-3} \text{ [Hz]} \\ 1.5 \times 10^{-12} f^{-3} \text{ [m}^2\text{/Hz]} \\ \qquad \text{for} \quad 1.0 \times 10^{-3} \leqq f \leqq 1.0 \times 10^{+2} \text{ [Hz]} \\ 1.5 \times 10^{-6} f^{-6} \text{ [m}^2\text{/Hz]} \\ \qquad \text{for} \quad 1.0 \times 10^{+2} \leqq f \leqq \infty \text{ [Hz]} \end{cases} \tag{3}$$

where the frequency f is to be inserted in hertz. This PDS is plotted in Fig. 1.

2.3.2 *Angle Scale Function, S_α*

The PDS of random tropospheric angle (α) errors for a single antenna radar are obtained from the range model PDS by operating on $P_m\{f\}$ with the angle scale function, S_α. The derivation of this function is based upon the fact that refractivity anomalies of characteristic length l, or of wavenumber κ, which drift through the LOS with the effective wind speed u_m cause random error components of frequency

$$f = u_m/l = \kappa u_m/2\pi. \tag{4}$$

To simplify the analysis the circular antenna aperture of diameter d is now approximated by an interferometer system of equal angle accuracy and baseline length

$$B = 0.626\, d \tag{5}$$

which lies in the plane of the angle being measured. The angle measurement is thought to be indirectly obtained by a range-difference (or phase-difference) measurement across the effective baseline length B. The tropospheric refractivity anomalies disturb this range-difference measurement to an amount that depends on the characteristic length l and on the antenna diameter d.

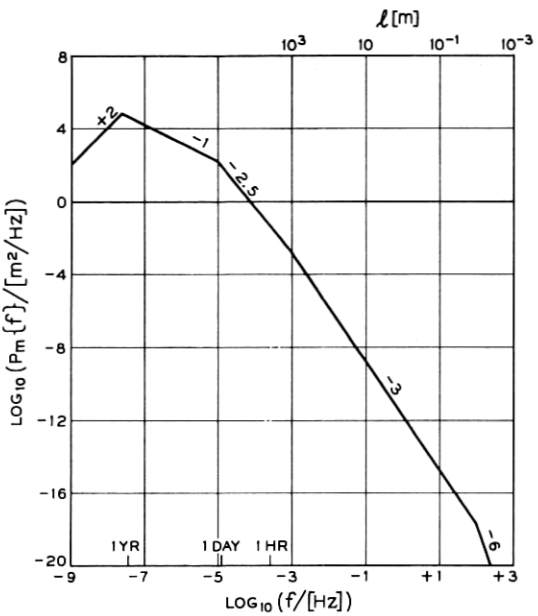

Fig. 1 — Model power density spectrum, $P_m\{f\}$, of tropospheric random errors in the range coordinate versus error-frequency, f, in a log-log plot. $P_m\{f\}$ is valid for the model conditions in Section 2.3.1. The tropospheric anomalies have the characteristic length l.

It is found that for relatively short characteristic lengths

$$l \leqq l_1 = 2d \tag{6}$$

which cause the high error frequencies

$$f \geqq f_1 = u_m/l_1 = 0.5\, u_m/d \tag{7}$$

the random range errors due to these anomalies at the two ends of the effective baseline length B are practically uncorrelated with each other. Thus, they cause a power density of the random error in the range-difference measurement that is twice as large as that of the random error in a single range measurement. Analytically, this finding may be expressed with the aid of a range-difference scale function

$$S_{\Delta R} = 2 \quad \text{for} \quad f \geqq f_1 = 0.5\, u_m/d. \tag{8}$$

The tropospheric refractivity anomalies with characteristic lengths larger than the critical length l_1, namely

$$l \geqq l_1 = 2d \tag{9}$$

cause the lower error frequencies

$$f \leqq f_1 = u_m/l_1 = 0.5\, u_m/d. \tag{10}$$

In this frequency region, the induced random range errors at the two ends of the effective baseline B are more and more correlated as the characteristic length is increased. It is found that with respect to the range-difference errors across B the antenna behaves like a high pass filter with break frequency f_1. Analytically, the resulting reduction in the power density of the low frequency random range-difference errors may be expressed by another branch of the range-difference scale function, namely

$$S_{\Delta R} = 2(f/f_1)^2 \quad \text{for} \quad f \leqq f_1 = 0.5\, u_m/d. \tag{11}$$

The multiplication of the range model PDS, $P_m\{f\}$, with the two branches of $S_{\Delta R}$ in their respective frequency regions would result in a PDS for the random tropospheric range-difference errors across the baseline B under model conditions.[7]

The last step in the derivation of the desired angle scale functions is based upon the assumption of small angular deviations relative to the axis of the antenna system. Then the angle error α is simply related to the range-difference error ΔR and the effective baseline length B by

$$\alpha = \Delta R/B. \tag{12}$$

In terms of power densities, this relation permits the calculation of the angle scale function S_α from the range-difference scale function $S_{\Delta R}$ and B, in general, as

$$S_\alpha = S_{\Delta R}/B^2. \tag{13}$$

The combination of (5), (8), (11), and (13) finally yields the angle scale functions in two branches, namely

$$\left.\begin{aligned} S_\alpha &= 20\ (f/u_m)^2 \quad \text{for} \quad 0 \leqq f \leqq f_1 \\ S_\alpha &= 5/d^2 \qquad\quad \text{for} \quad f_1 \leqq f \leqq \infty \end{aligned}\right\}. \tag{14}$$

The breakfrequency of the angle scale function is

$$f_1 = 0.5\, u_m/d, \tag{15}$$

where $u_m = 1$ [m/sec] is the model wind speed taken normal to the LOS and in the plane of the angle measurement, and d is the diameter of the circular antenna aperture.

2.3.3 *Aperture Smoothing Function,* Φ_α

The spatial smoothing on tropospheric random error components that are due to refractivity anomalies of small characteristic length ($l \ll d$) is another function of the antenna diameter, d. Here the combined effects of several small refractivity anomalies tend to cancel across the antenna aperture, hence the antenna acts like a low-pass filter in the error-frequency $\{f\}$-domain. A simplified aperture smoothing function which analytically represents this effect is

$$\left.\begin{aligned} \Phi_\alpha &= 1 \qquad \text{for} \quad 0 \leqq f \leqq f_2 \\ \Phi_\alpha &= (f_2/f)^2 \quad \text{for} \quad f_2 \leqq f \leqq \infty \end{aligned}\right\}, \tag{16}$$

where

$$f_2 = 2\, u_m/d \tag{17}$$

is the breakfrequency for aperture smoothing in angle measurements.

2.3.4 *Effective Path Length Function,* Λ

From theories of propagation through a uniformly turbulent random medium, as for example given by Chernov,[1] it is known that the variance of phase, range and related errors is proportional to the path length. This proportionality holds in both the near-field and the far-field regions of the "scattering" refractivity anomalies of a given characteristic length, l. Therefore, it is possible to account for an effective tropospheric path length, L, which is different from the model path length L_m, by multiplying the power density with the effective path length function

$$\Lambda = L/L_m \quad \text{for} \quad 0 \leqq f \leqq \infty. \tag{18}$$

The required effective tropospheric path length, L, may be calculated by integrating over the geometrical length differentials along the LOS, which are weighted with the square of the local average refractivity at the height of each layer of the atmosphere. The necessary data on the variation of the refractivity with height have been taken from Bean and Thayer.[8] If the height of the target is $h_2 \geqq 10$ [km] above the surface of the Earth, and the apparent elevation angle is $E_a \geqq 3°$, the effective tropospheric path length becomes

$$L = L_o/\sin E_a\,, \tag{19}$$

where

$$L_o = \left(\frac{N_s}{N_m}\right)^2 (6.61 - 0.01N_s)[\text{km}] \tag{20}$$

is the effective height of the troposphere for surface refractivities

$$250 \leqq N_s \leqq 450,$$

and N_m is the model surface refractivity.

In this case, which is relevant to many radar and optical tracking tasks, one thus has the effective path length function as

$$\Lambda = \frac{(N_s/N_m)^2}{L_m \cdot \sin E_a} (6.61 - 0.01N_s)[\text{km}] \quad \text{for} \quad 0 \leqq f \leqq \infty. \quad (21)$$

2.3.5 *Weather Functions, W*

As stated in paragraph 2.3.1 the model power density spectrum, $P_m\{f\}$, is defined as the *lower* limit of the available observations normalized to the model conditions. Essentially all (say 99 percent) normalized observations exhibit larger errors than given by P_m. Consequently, all PDS directly derived from $P_m\{f\}$ for other coordinates and tracking situations also would only give the expected *minimum* errors. Since it is frequently desired to state more about the expected distribution of the derived PDS above the expected minimum level we have introduced certain power gain functions, called weather functions, W_q. These are defined as the maximum weather function $W_{\max}\{f\}$ which covers the maximum errors previously observed, and the median weather function $W_{\text{med}}\{f\}$. On a "global" basis (actually only embracing all circumstances of previous observations entered into the model data), it is expected that 50 percent of the measured PDS will lie above and below the PDS predicted with $W_{\text{med}}\{f\}$, and essentially all (say 99 percent) of the measured PDS will lie below the PDS predicted with $W_{\max}\{f\}$.

The maximum weather function derived from available observations[4, 5, 6, 7] is

$$W_{\max}\{f\} = \left\{ \begin{array}{ll} 6 \text{ for} & 0 \leqq f \leqq 1.00 \times 10^{-5} \text{ [Hz]} \\ 1.89 \times 10^{+8} f^{+1.5} & \\ \quad \text{for} & 1.00 \times 10^{-5} \leqq f \leqq 2.23 \times 10^{-5} \text{ [Hz]} \\ 20 \text{ for} & 2.23 \times 10^{-5} \leqq f \leqq 1.00 \times 10^{-3} \text{ [Hz]} \\ 6.32 \times 10^{+2} f^{+0.5} & \\ \quad \text{for} & 1.00 \times 10^{-3} \leqq f \leqq 1.00 \times 10^{-1} \text{ [Hz]} \\ 200 \text{ for} & 1.00 \times 10^{-1} \leqq f < \infty \text{ [Hz]} \end{array} \right\} \quad (22)$$

where f is in hertz.

The median weather function is taken as

$$W_{\text{med}}\{f\} = (W_{\max}\{f\})^{0.5}. \tag{23}$$

Both functions are plotted in Fig. 2. Note that $W_{\min} = 1$ by definition.

2.3.6 *Effective Wind Functions, U*

The purpose of the effective wind functions, U, is to introduce other magnitudes of effective wind speed, $u_\alpha \neq u_m$, into the model. The derivation of these effective wind functions rests upon the assumption that an isotropic, frozen turbulence field of refractivity anomalies exists in the troposphere which moves through the LOS with a constant effective wind speed component, u_α, normal to the LOS and in the plane of the angle coordinate α. With this assumption, a given anomaly causes an angle error of a magnitude that is independent of u_α, and of a frequency

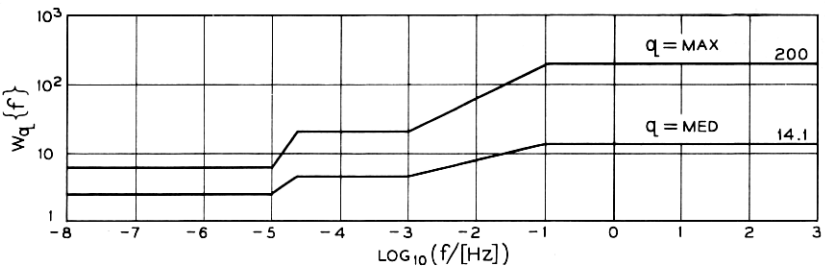

Fig. 2 — Maximum and median weather functions, $W_{\max}\{f\}$ and $W_{\text{med}}\{f\}$, respectively, versus decadic logarithm of the error frequency, f.

that is proportional to u_α. It was found that a PDS that is given in $\{f,u_m\}$-space as a sum of branches of the form

$$P_\alpha'\{f,u_m\} = P_o'(f/f_o)^\gamma \quad \text{for} \quad f_{m,\min} \leqq f \leqq f_{m,\max} \tag{24}$$

is transformed into an equivalent PDS in $\{f,u_\alpha\}$-space by the relations

$$\left.\begin{aligned} P_\alpha''\{f,u_\alpha\} &= U_P \cdot P_\alpha'\{f,u_m\} \\ \text{for} \qquad & \\ U_f \cdot f_{m,\min} = f_{\alpha,\min} \leqq f \leqq f_{\alpha,\max} &= U_f \cdot f_{m,\max} \end{aligned}\right\}, \tag{25}$$

where the effective wind function for the transformation of the power density is

$$U_P = (u_m/u_\alpha)^{\gamma+1} \tag{26}$$

and the effective wind function for the transformation of the frequency regions

$$U_f = u_\alpha / u_m \,. \tag{27}$$

In these relations the $f_{\alpha,\min}$ and $f_{\alpha,\max}$ are the limits of the frequency region in which P_α'' is valid after the transformation to $\{f,u_\alpha\}$-space.

In the special case of small angular velocity of the LOS, the equivalent wind due to the angular rate is negligible compared to the natural winds in the atmosphere. The effective wind speed is then simply

$$u_\alpha = w_\alpha \,, \tag{28}$$

where w_α is that component of the natural wind which is normal to the LOS and in the plane of the angle α. In this plane of the angle α, the atmospheric refractivity anomalies, on the average, appear to move through the LOS with the speed w_α.

The calculation of the effective wind speed for azimuth ($\alpha \rightarrow A$) angle errors depends on the geometrical relations between the LOS and the natural average wind vector, $\hat{w}$, Fig. 3. If A is the azimuth angle of the LOS, and δ is the azimuth of the wind vector, their difference

$$\beta = \delta - A \tag{29}$$

can be used to calculate the effective wind speed for azimuth angle errors

$$u_A = | w_A | = | \hat{w} | \cdot | \sin \beta | . \tag{30}$$

With the horizontal LOS component (see Fig. 3)

$$w_1 = | \hat{w} | \cdot \cos \beta \tag{31}$$

the effective wind speed for elevation errors similarly becomes, Fig. 4,

$$u_E = | w_E | = | w_1 | \cdot | \sin E_s | \tag{32}$$

or

$$u_E = | \hat{w} | \cdot | \cos \beta \cdot \sin E_s | . \tag{33}$$

Only the magnitudes of the effective wind speeds are of interest in this special case of small angular velocity of the LOS, and a single-site radar.

2.4 *Computation of the Predicted PDS*

In the prediction of the PDS of random tropospheric angle errors for a particular tracking situation numerical values are inserted for all independent parameters in the model functions given above. The range model PDS, $P_m\{f\}$, is then multiplied by the model functions, within the limits of the stated frequency regions, in the following sequence: angle scale

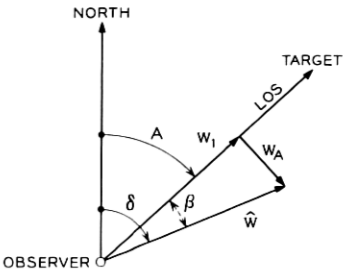

Fig. 3 — Horizontal projection of LOS, wind vector $\hat{w}$, and azimuth angle A.

function, aperture smoothing function, effective path length function, weather function, and effective wind functions.

For the tracking situation of the Early Bird observations on May 7, 1965 the numerical values for the parameters and model functions are given in the Appendix. The operation of these models functions on the range model PDS, $P_m\{f\}$, resulted in four PDS, namely a predicted minimum spectrum and a predicted maximum spectrum for each of the two angle coordinates azimuth and elevation. The resulting PDS $P_{A,\min}$, $P_{A,\max}$ and $P_{E,\min}$, $P_{E,\max}$ are plotted over the interesting frequency range in Figs. 12, and 13.

III. OBSERVATIONS OF RANDOM TROPOSPHERIC ANGLE ERRORS ON THE EARLY BIRD SATELLITE

3.1 *Data Acquisition*

3.1.1 *Method and Equipment*

For the acquisition of the data on random angle variations in azimuth and elevation, the apparent position of the microwave beacon (frequency about 4000 MHz) of the Early Bird satellite was measured with the horn

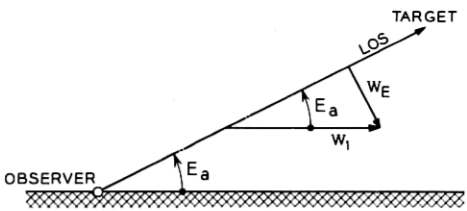

Fig. 4 — Projection of wind vector into vertical plane through LOS with apparent elevation angle E_a.

antenna (aperture diameter $d = 67.7$ ft) and its associated equipment. During these measurements the communications carrier of the satellite was switched off; this resulted in an increase in beacon signal strength to such a level that the thermal receiver noise in the obtained angle measurements was negligible compared to the desired tropospheric random errors.

The signal flow through the major pieces of equipment which were used is illustrated in Fig. 5. After acquisition of the Early Bird satellite beacon in the main beam (beamwidth $\theta = 0.225$ deg) of the horn antenna, the antenna control was turned over to the vernier autotrack system, and the servo loop opened by switching off the hydraulic drive motors. The antenna was now fixed in an orientation indicated by the digital display of the azimuth (A) and elevation (E) angles given in degrees, and derived from digital data pickoff units, which have a precision of encoding[11] of 0.00275[deg].

The satellite now appeared to drift through the fixed horn antenna beam in an irregular motion, which was partially due to motion in its true position (orbit), but also due to the refractive index variations in the intervening atmospheric propagation medium, and possibly other disturbances. The apparent angular position of the satellite relative to the electrical axis of the horn antenna on the ground was determined by the autotrack system which contains angle error sensing and processing equipment. The azimuth and elevation error signals, $\Delta A\{t\}$ and $\Delta E\{t\}$ from the autotrack system were passed through low-pass recording filters before recording either by oscilloscope and camera, or by analog strip chart recorder.

The photographic pictures of the oscilloscope display giving ΔA vs ΔE were only used for inspection. The strip chart recordings giving the $\Delta A\{t\}, \Delta E\{t\}$ time series, however, were used for the more detailed analysis of the data, as described later.

3.1.2 *Propagation Path and Mean Satellite Motion*

During the measurements the propagation path pointed from the horn antenna near Andover, Maine, to the Early Bird satellite approximately at an azimuth angle $A \approx 128.5°$ (southeast), and an elevation angle $E \approx 24.5°$. The slant range between ground antenna and satellite was about 24,300 [statute miles] $\approx$ 39,100 [km]. The terrain surrounding the Earth Station may be described as a shallow bowl of perhaps 10-miles diameter surrounded by hills of up to about 3.5 [deg] elevation.

The mean apparent satellite motion with respect to the azimuth and elevation angles given above consisted of (i) a small linear drift with an

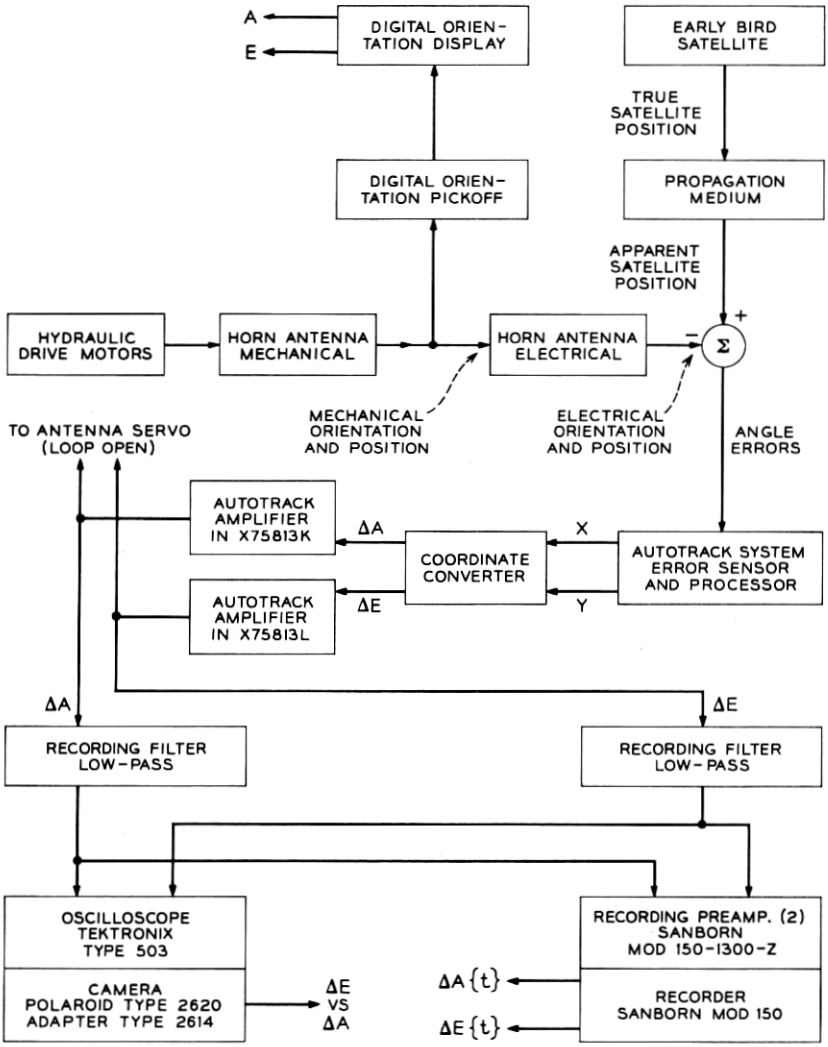

Fig. 5 — Flow diagram of data acquisition.

azimuth component of $\dot{A}_1 = -2.08 \times 10^{-3}$ [deg/hr], and an elevation component of $\dot{E}_1 = -1.22 \times 10^{-3}$ [deg/hr], plus (*ii*) a diurnal elliptical motion with peak-to-peak amplitudes of $\hat{A} = 0.266$ [deg] in azimuth and $\hat{E} = 0.245$ [deg] in elevation. The net result of these components appears at the Earth Station as a slow motion of the satellite along a helical path seen under an oblique angle. This picture of the mean apparent satellite

motion was obtained by plotting the hourly azimuth and elevation angles from the digital display for a few days before the analyzed random angle error data were recorded. The random azimuth and elevation angle errors, ΔA and ΔE, which are subjects of this paper are superimposed on this mean apparent motion.

3.1.3 *Date and Time of Observations*

The random angle error data recorded on strip charts, and analyzed in this paper were taken on May 7, 1965 between about 23 hr:38 min EDT and 23 hr:59 min EDT.

3.1.4 *Weather Conditions*

Weather data at the horn antenna of the Andover Earth Station were not taken. However, the weather data may be estimated from those taken at a private station in nearby Rumford, Me. This estimation yields the following data:[18] Cloud cover 9/10, wind South 19 [statute miles/hr], dry bulb temperature 41.8 [°F], dew point 35 [°F], and pressure 28.5 [inches] = 965.0 [millibars].

3.1.5 *Recording Filters*

The low-pass recording filters mentioned in Section 3.1.1 above were simple two-section RC filters. Since the source impedances feeding these filters are small, and the load impedances connected to their outputs are large compared to the resistances in the RC sections of the filters, their inverse power gain is

$$F = G^{-1} \approx 1 + (\omega T)^2 ((\omega T)^2 + 7).$$

In this equation, F is the ratio of input power to output power, $T = RC$ is the time constant of one filter section, and $\omega = 2\pi f$, where f is the frequency.

The power density of the random angle errors before the filters may then be obtained by multiplying the power density of the recorded random angle errors with the inverse power gain F. The filters which were used in these observations allowed a choice between two cutoff frequencies. The results of numerical calculations of the inverse power gains versus frequency for the "LOW", and "HIGH" filters are plotted in Fig. 6.

3.1.6 *Calibration*

The sensitivities of the recorded error voltages (after the recording filters) to errors in the azimuth and elevation angles with respect to the

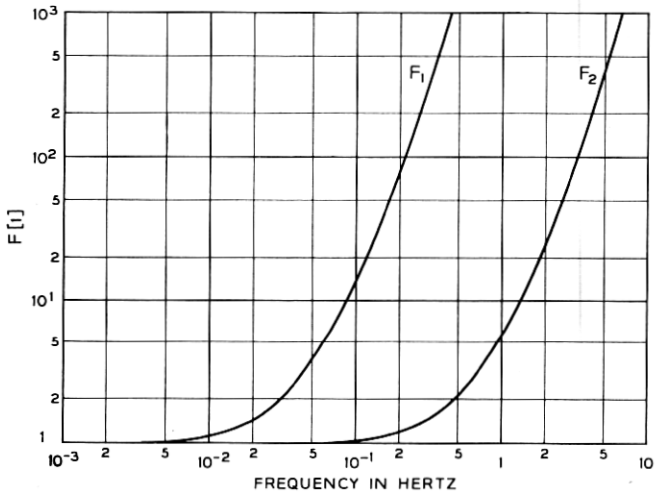

Fig. 6 — Inverse power gain, F, of recording filter versus frequency, f. F_1 for filter in "LOW" range. F_2 for filter in "HIGH" range.

electrical axis of the horn antenna were obtained by direct calibration on the Early Bird satellite. For this purpose, the antenna servo system was disabled, and manual angle offsets were then inserted and their effects on the strip chart records were measured.

3.1.7 *Oscilloscope Displays*

Photographs of oscilloscope displays of the random elevation error (ΔE) versus the simultaneously occurring random azimuth error (ΔA) were also made.

The photo tracing in Fig. 7 was obtained at 22:30 EDT May 7, 1965 while the recording filters were in the "HIGH" range, and the exposure time was five seconds. It is obvious that in this sample of the higher frequency errors the peak-to-peak azimuth variations (about 40 microradians) are considerably larger than those of the elevation errors (20 microradians).

The photo tracing in Fig. 8 was taken at 22:38 EDT on the same date with the recording filters in the "LOW" range. The exposure time was two minutes. In this sample of the lower frequency errors the peak-to-peak azimuth variations (12 microradians) are slightly smaller than the elevation variations (18 microradians).

As mentioned before, these photos were only used for inspection and not for numerical analysis.

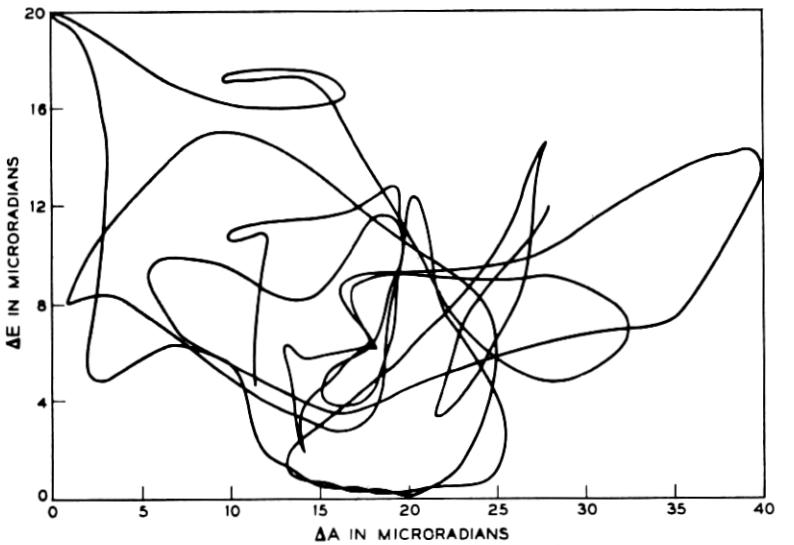

Fig. 7 — Tracing of oscilloscope photograph of random elevation error (ΔE) versus random azimuth error (ΔA). Time is the parameter. Recording filters in "HIGH" range. Exposure time: five seconds.

3.2 *Data Processing and Analysis*

3.2.1 *General Methods and Equipment*

The data on azimuth (ΔA) and elevation angles (ΔE) versus time were recorded on a strip chart recorder with the recording filters in the "LOW" range. The time series of azimuth and elevation angles were manually digitized at two second intervals.

After the manual digitizing process the time series of azimuth and elevation variations were punched into cards for subsequent processing on the 7094 digital computer.

3.2.2 *Time Series of Observed Angle Variations*

The time series of the azimuth (ΔA) and elevation (ΔE) angle variations are shown in Figs. 9 and 10, respectively.

The total observation time was somewhat above twenty minutes. This observation time was limited by the mean apparent drift of the satellite in the fixed antenna beam. This drift resulted in the recording traces going off scale after a certain time.

A total of 720 azimuth data points, and 666 elevation data points were

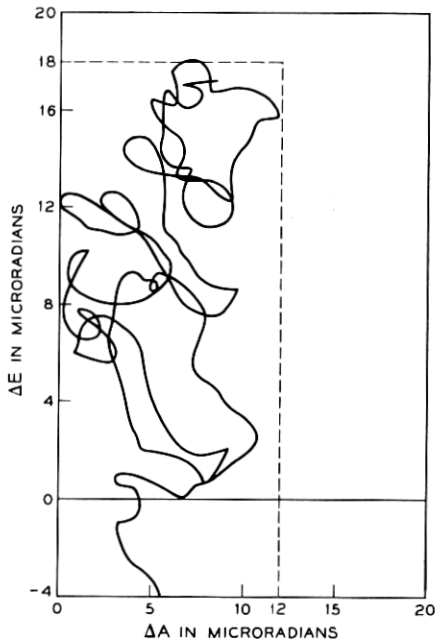

Fig. 8 — Tracing of oscilloscope photograph of random elevation error (ΔE) versus random azimuth error (ΔA). Time is the parameter. Recording filters in "LOW" range. Exposure time: two minutes.

recorded. Due to the systematic drift the elevation record went off the recording scale sooner than the azimuth record.

3.2.3 *Power Density Spectra of Observed Angle Variations*

The random variations of the observed azimuth and elevation angles will also be described by their power density spectra (PDS) for comparison with the predictions. The numerical computation of the PDS from the time series of data is made on a digital computer by the indirect method described by Blackman and Tukey.[17] It proceeded in the following steps: calculation and removal of the mean, and of the linear trend in the series; tapering the first 5 percent (start) and the last 5 percent (end) of the time series with a cosine function; computation of the autocorrelation function versus number r of $0 \leqq r \leqq M$ time lags each of duration of the sampling period Δt; computation of the Fourier transform of the autocorrelation function by a cosine series resulting in a raw power spectrum and subsequent smoothing of the raw spectrum by sliding,

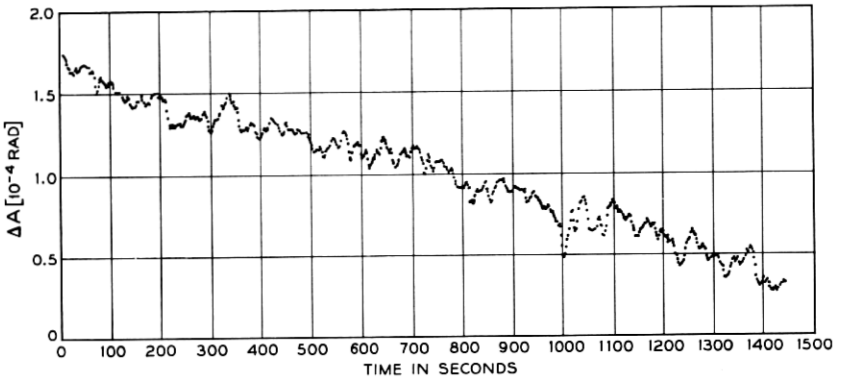

Fig. 9 — Time series of observed azimuth angles, ΔA, versus time, t.

weighted averages of values for three neighboring frequency steps with weights 0.25, 0.50, and 0.25.

The computer program actually calculates a quantity $X'\{f\}$, called "power spectrum", which is related to the usual power density spectrum $P'\{f\}$ by the equation

$$P'\{f\} = X'\{f\}/\Delta f, \tag{34}$$

where

$$\Delta f = f_N/M = 1/(2\cdot\Delta t\cdot M) \tag{35}$$

and

f_N = Nyquist frequency
M = maximum number of lags in autocorrelation
Δt = sampling period.

In this equation, the primed quantities indicate that they still refer to the data at the *output* side of the recording filter. In order to obtain the desired power density spectrum at the *input* of the recording filter, $P'\{f\}$ must be multiplied by the inverse power gain of the filter, $F\{f\}$, yielding

$$P\{f\} = 2\cdot\Delta t\cdot M\cdot F\{f\}\cdot X'\{f\}. \tag{36}$$

Additional smoothing of the power density spectrum is used at the higher error-frequencies, since many cycles of these angle error components have been observed. This is done with a filter of approximately constant relative bandwidth, $\beta = b/f = 0.231$, at the expense of absolute

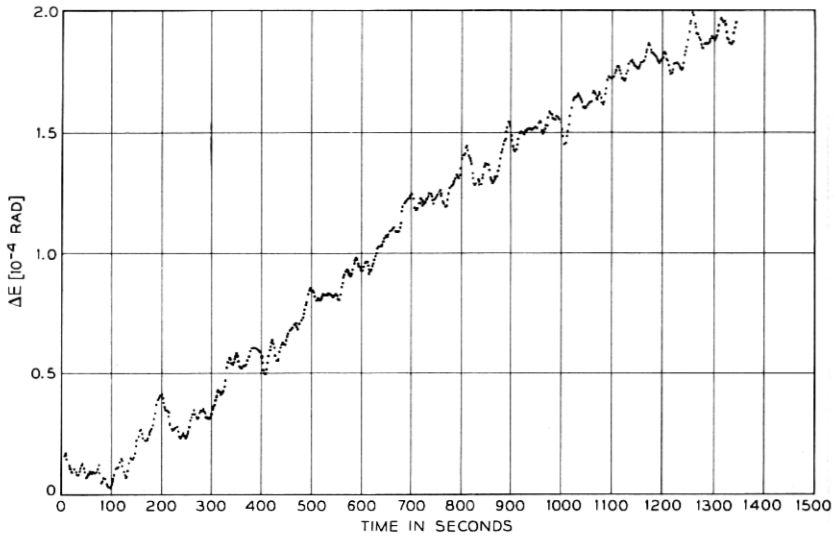

Fig. 10 — Time series of observed elevation angles, ΔE, versus time, t.

frequency resolution. This point will be illuminated again in Section 3.2.4.

The data on azimuth and elevation angle variations given in Section 3.2.2 were analyzed with the methods just described. It was found that the mean linear trends during these observations were in azimuth $+8.1 \times 10^{-8}$ [rad/sec], and in elevation -1.7×10^{-7} [rad/sec]. Even at a distance of 10 [km] along the line-of-sight the magnitude of these angular rates amount to beam sweeping speeds of less than 0.002 [m/sec], which are indeed negligible compared to natural wind speeds in the troposphere.

The power density spectra of the observed azimuth and elevation variations at the input of the recording filters, $P_A\{f\}$ and $P_E\{f\}$, which result from these calculations are plotted in Figs. 12 and 13, respectively. Other spectra also plotted in these figures are explained below.

3.2.4 *Confidence Limits for Power Density Spectra*

In computing confidence limits for the power density spectra it is necessary to distinguish between two error-frequency regions: the low-frequency region in which the absolute analyzing bandwidth of the PDS calculation

$$b = (M \cdot \Delta t)^{-1} \tag{37}$$

is constant, and the high-frequency region in which the relative analyzing bandwidth

$$\beta = b/f \tag{38}$$

is constant.

In the low-frequency region, with constant absolute analyzing bandwidth, b, the number of degrees of freedom in the PDS estimate is approximately

$$k = 2N/M \tag{39}$$

where N is the number of data points observed.

In the high-frequency region, with constant relative analyzing bandwidth, β, the number of degrees of freedom is frequency dependent according to

$$k = 2\beta f N \cdot \Delta t. \tag{40}$$

The confidence limits for the calculated PDS of the observations can now be given, the lower limit being

$$P_1\{f\} = P\{f\}/K_1\{f\} \tag{41}$$

and the upper limit

$$P_2\{f\} = K_2\{f\} \cdot P\{f\}, \tag{42}$$

where $P\{f\}$ is the calculated PDS, and $K_{1,2}\{f\}$ are the confidence factors.

For a confidence level of $\rho = 95$ percent the *upper confidence factor* is approximately

$$K_2 = 1 + \frac{2.77}{\sqrt{k-1}} + \frac{1.30}{k-1}, \tag{43}$$

the *total confidence factor* (here only used as an intermediate to obtain K_1)

$$K_{21} = \text{antilog}_{10}\left(\frac{2.40}{\sqrt{k-1}}\right), \tag{44}$$

and the *lower confidence factor*

$$K_1 = K_{21}/K_2, \tag{45}$$

where k is the number of degrees of freedom given above. For $k \geqq 5$ the stated analytical approximations for the confidence factors have less than 10 percent error.

The resulting numerical values for the upper (K_2) and lower (K_1) confidence factors are plotted in Fig. 11. The results of calculating the

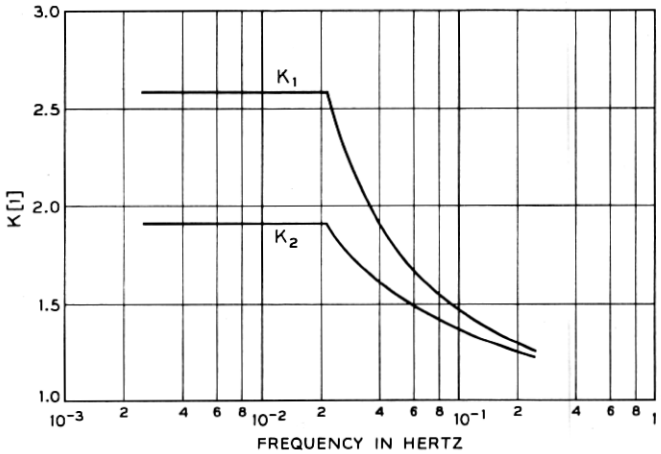

Fig. 11 — Relative confidence factors, K_1 and K_2, for ρ = 95 percent confidence level versus frequency, f.

upper confidence limits (P_{A2}, P_{E2}), and the lower confidence limits (P_{A1}, P_{E1}) for the azimuth (P_A) and elevation (P_E) spectra are plotted in Figs. 12 and 13.

3.2.5 *Chart Reading Error*

The errors which are introduced into the data by the manual reading of strip chart records (digitizing) are of the same type as quantization errors. The variance due to a given quantization step size (q) is known to be[19]

$$\sigma_q^2 = q^2/12. \tag{46}$$

If it is now assumed that the quantization noise, which causes this variance, is sharply bandlimited white noise of constant power density (P_q'), and with a cutoff frequency equal to the folding frequency of the digitized time series (f_N), then one also has the variance as

$$\sigma_q^2 = \int_0^{f_N} P_q' \cdot df = P_q' \cdot f_N . \tag{47}$$

Consequently, the noise power density due to the manual chart reading is

$$P_q' = \sigma_q^2/f_N = q^2 \cdot \Delta t/6. \tag{48}$$

As before, this primed power density is taken at the output side of the

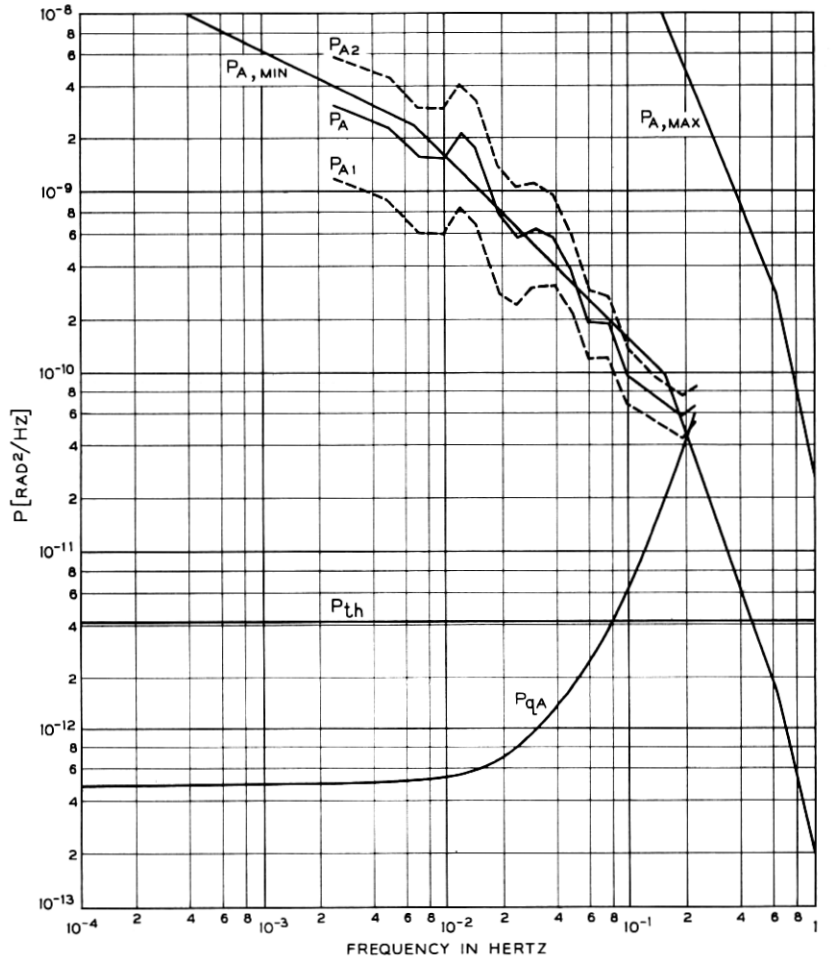

Fig. 12 — Power density of random azimuth angle errors, P, versus frequency, f. P_A, P_{A1}, P_{A2} = observed PDS and 95 percent confidence limits; $P_{A,\min}$, $P_{A,\max}$ = predicted tropospheric PDS limits; P_{th} = thermal receiver noise; P_{qA} = manual chart reading error.

low-pass recording filter. In order to obtain the power density spectrum of the chart reading error referred to the input of the recording filter, it is necessary to multiply P_q' with the inverse power gain $F_1\{f\}$ of the filter, see Section 3.1.5, which yields here for the azimuth coordinate

$$P_{qA}\{f\} = F_1\{f\} \cdot P_{qA}' = F_1\{f\} \cdot q_A^2 \cdot \Delta t/6 \tag{49}$$

and for elevation

$$P_{q_E}\{f\} = F_1\{f\} \cdot P_{q_E}' = F_1\{f\} \cdot q_E^2 \cdot \Delta t/6. \quad (50)$$

The effective quantization step size for azimuth was $q_A \approx 1.2$ microradians, and for elevation $q_E \approx 0.88$ microradians, the difference being due to different scale factors in the two channels. The sampling period as stated before was $\Delta t = 2$ seconds. The resulting PDS of the manual digitizing process, P_{q_A} and P_{q_E}, are also plotted in Figs. 12 and 13.

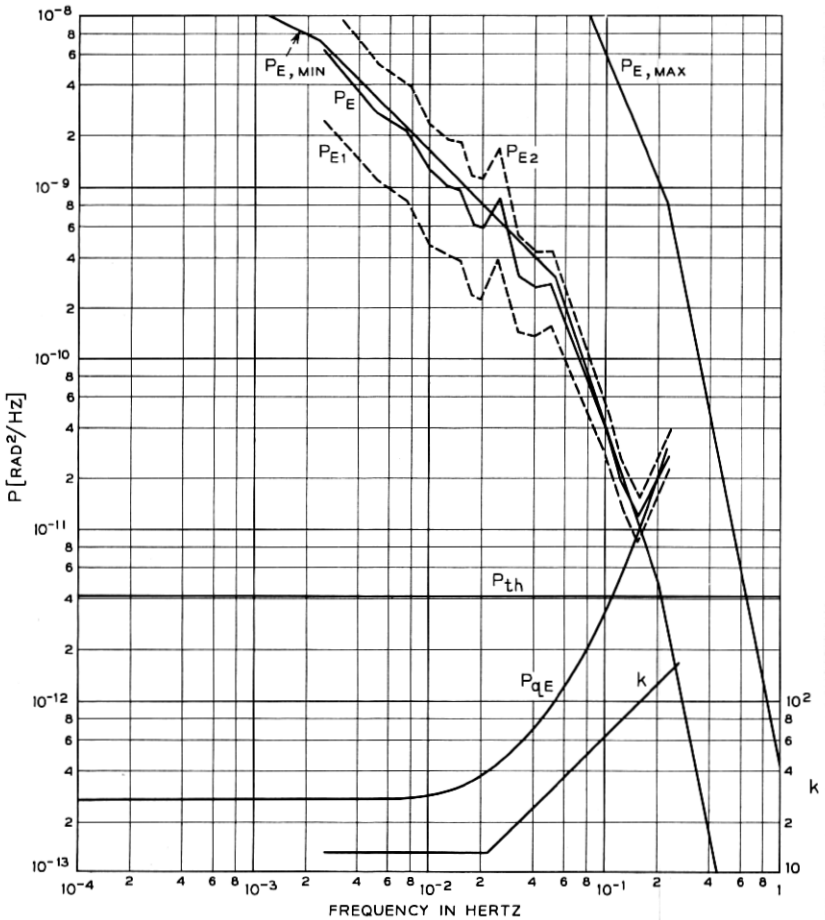

Fig. 13 — Power density of random elevation angle errors, P, versus frequency, f. P_E, P_{E1}, P_{E2} = observed PDS and 95 percent confidence limits; $P_{E,\min}$, $P_{E,\max}$ = predicted tropospheric PDS limits; P_{th} = thermal receiver noise; P_{qE} = manual chart reading error; k = number of degrees of freedom.

3.2.6 *Thermal Angle Errors*

During observations of the tropospheric random angle errors it is important to keep angle errors due to thermal receiver noise at a comparatively low level. The variance of thermal angle errors may be obtained[20] as

$$\sigma_{th}^2 = \frac{\theta^2\left(1+\frac{S}{N}\right)}{8\left(\frac{S}{N}\right)^2 B\tau} \tag{51}$$

which can be reduced for $S/N \gg 1$ to

$$\sigma_{th}^2 = \frac{\theta^2}{8B\tau\,(S/N)}, \tag{52}$$

where

θ = antenna beamwidth
S/N = input signal-to-noise power ratio
B = receiver bandwidth
τ = post-detection integration time.

In order to derive the power density (P_{th}) of the white thermal noise spectrum it is first recognized that the variance of the thermal angle error is also

$$\sigma_{th}^2 = \int_0^\infty \frac{P_{th}df}{1+(f/f_c)^2}, \tag{53}$$

where

$$f_c = 1/2\tau \tag{54}$$

is the cut-off frequency of the post-detection low-pass filter. Equation (53) may be integrated with the substitution $x = f/f_c$; $df = f_c\,dx$ giving

$$\sigma_{th}^2 = P_{th}\cdot f_c\cdot \arctan\,(f/f_c)\,\Big|_0^\infty \tag{55}$$

or

$$\sigma_{th}^2 = \frac{\pi}{2} f_c\cdot P_{th}\,. \tag{56}$$

Combining (52), (54), and (56) then yields the desired density of the thermal angle noise as

$$P_{th} = \frac{\theta^2}{2\pi B(S/N)} \tag{57}$$

independent of the frequency f.

During the observations on May 7, 1965, which are analyzed in this report, the measured signal-to-noise ratio was $(S/N)' = 23$ [dB] = 200[1] while the communications carrier of the Early Bird satellite was switched off. (This ratio was $(S/N)' = 13$ [dB] = 20 [1] due to a weaker beacon signal when the carrier was on.) The primed signal-to-noise ratios stated here are referred to a 3-kHz bandwidth. The effective noise bandwidth, however, is considerably lower due to the employment of a phase-locked tracking loop quite like the one described in Ref. 15. From Fig. 12 in that reference it is seen that the noise bandwidth for

$$(S/N)' = 23 \text{ [dB]} \quad \text{is} \quad B = 390 \text{ [Hz]},$$

which further results in an effective signal-to-noise ratio

$$S/N = 200 \times (3{,}000/390) = 1{,}538 \text{ [1]}.$$

Since the antenna beamwidth was $\theta = 0.225° = 3.94 \times 10^{-3}$ [rad] the desired power density of the thermal receiver noise with (57) here becomes $P_{th} = 4.1 \times 10^{-12}$ [rad^2/Hz] while the communications carrier is switched off, and the beacon signal is strong. This thermal noise level in the angle measurements was low enough to permit observation of the random tropospheric angle variations up to frequencies of a few 0.1 [Hz], see Figs. 12 and 13.

IV. COMPARISON BETWEEN PREDICTED AND OBSERVED ANGLE ERRORS

The comparison between predicted, and observed power density spectra of random tropospheric angle variations may now be made with the aid of Figs. 12 and 13 into which all relevant spectra have been entered. The observed spectra (P_A , P_E) resulted from the analysis of random angle error data taken on the Andover Horn to Early Bird path on May 7, 1965 between about 23 hr:38 min EDT, and 23 hr:59 min EDT. An inspection of Figs. 12 and 13 shows that the PDS of the observations cover about two decades of frequency, namely

$$2.50 \times 10^{-3} \text{ [Hz]} \leqq f \leqq 0.25 \text{ [Hz]}.$$

The comparison of the observed PDS (P_A ; P_E) with their respective predicted PDS ($P_{A,\min}$, $P_{A,\max}$; $P_{E,\min}$, $P_{E,\max}$) yields almost identical results for the two angle oocrdinates azimuth (A) and elevation (E). In particular it is found that the PDS of the observed random angle

variations (P_A ; P_E), within their respective 95 percent confidence limits (P_{A1} , P_{A2} ; P_{E1} , P_{E2}), lie almost exactly on the predicted *minimum* power spectra ($P_{A,\min}$; $P_{E,\min}$) for random *tropospheric* angle errors.

Thus, the observed PDS match the predicted PDS quite well in the *shape* of their frequency dependence. The *low level* of the observed PDS relative to the predicted range of PDS is thought to be due to the "good tracking weather" at the Andover, Maine site and at the particular time of observation (a quiet night). It must be remembered here that the prediction is based mainly upon the NBS range and phase measurements[4,5,6,7] which were obtained in Hawaii and Colorado. Whether the low level of the random tropospheric errors observed in Maine is a permanent property of the site, or a chance occurrence can be decided by the analysis of additional observations.

It is also possible to compare the observed PDS of the azimuth errors with that of the elevation errors. It is found that the azimuth errors here have a higher level at frequencies $f > 0.1$ Hz than the elevation errors; this is an effect of the higher azimuth wind speed component ($u_A = 6.7$ m/sec versus $u_E = 2.2$ m/sec). Even larger differences between the azimuth and elevation random errors are expected when their effective wind speed components differ by larger amounts. Such wind speed differences may be caused by either peculiar orientation of the natural wind vector relative to the line-of-sight, or also by differences in angular tracking rates.

Near the high-frequency end of the covered band the observed PDS deviate significantly in shape from the predictions. This deviation is particularly evident in the steep increase of the observed elevation PDS above $f = 0.15$ [Hz]. This increase is identified as an effect of quantization errors in the manual digitizing of the analog strip chart records. The transformation of these digitizing errors to the input side of the recording filters results in the steeply rising PDS (P_{qA} , P_{qE}) for these frequencies.

In the frequency band of the observations the angle errors due to thermal receiver noise have a PDS (P_{th}) which is negligible compared to that of the tropospheric angle errors, provided the communications carrier in the Early Bird satellite is turned off.

It is also possible to integrate the predicted PDS of the random tropospheric angle errors over the entire error frequency band, and then to take the square root to obtain the standard deviation

$$\sigma = \left(\int_0^\infty P df \right)^{\frac{1}{2}}.$$

When these integrals are calculated for the predicted minimum and maximum PDS, it is found that the standard deviations of the random tropospheric angle errors are expected to lie between $\sigma_{min} \approx 10$ [microradians] ≈ 2 [seconds of arc] and $\sigma_{max} \approx 65$ [microradians] ≈ 13 [seconds of arc]. This range of values compares quite well with Kennedy and Rosson's estimate that the tropospheric angle errors lie between 20 to 50 microradians.[20]

The standard deviation of the expected tropospheric angle fluctuations versus baseline length was previously calculated from NBS data on refractivity and range variations by D. K. Barton.[21] For the equivalent baseline length of the Andover horn antenna of about forty feet, Barton's graph shows a standard deviation of perhaps seventy microradians, a value slightly above our predicted maximum.

Some astronomical observations of random fluctuations in angular star positions, as quoted by Tatarski,[2] show standard deviations of one half to one second of arc. These observations have been made under conditions quite different from those for which our predictions are valid, namely with visible light, in clear weather, with smaller apertures, and probably only over a small fraction of the entire error frequency band. Therefore, it is not too surprising to find that these astronomical measurements lie below our minimum prediction.

Within the limitations of the analyzed observations, and of the described model it is concluded that the observed random angle variations are essentially due to random variations of the refractive index field in the troposphere. The feasibility of acquiring additional data on tropospheric angle errors with the Andover horn antenna on geo-stationary satellites of the Early Bird type therefore was also demonstrated. These data may now be obtained on a routine basis with available and operating equipment.

The comparison of the observations given in this paper with the prediction of random tropospheric angle errors gives some confidence in the described analytical model. Additional observations of random tropospheric angle errors were made with radar and optical equipment over other propagation paths. The comparison of these observations with the relevant predictions from the analytical model (not reported here) are also satisfactory, and have further strengthened the confidence in the model.

V. SUMMARY

Earth-based radar and optical systems which are used to measure the position (and its time derivatives) of both distant and near objects are

ultimately limited in accuracy by random angle variations caused by fluctuations of the tropospheric refractive index. For the analysis and synthesis of these systems an analytical model of the random tropospheric errors has been developed.

With this model, the predicted minimum and maximum power density spectra (PDS) between which observed PDS of tropospheric errors are expected to lie can be analytically calculated. The calculation is performed by operating with certain model functions, which depend on the tracking system parameters, on a model PDS (P_m) given in the range coordinate. P_m has been derived from observations of random variations in the tropospheric refractive index, and in range and phase measurements made mainly at the National Bureau of Standards.

A simplified analytical model of random tropospheric angle errors is described here, which is applicable to a tracking situation involving one (almost stationary) target and a single observer. This model is also used to predict the minimum and maximum PDS of the random tropospheric azimuth and elevation angle errors for microwave observations of the Early Bird geo-stationary communication satellite with the large horn-reflector antenna at the AT &T ground station near Andover, Maine.

The general method of data acquisition, Fig. 5, and the specific circumstances of some actual observations on the Early Bird satellite with the Andover horn are then described. Microwave azimuth and elevation angle measurements for an observation time of about twenty minutes were taken on May 7, 1965, while the Early Bird satellite appeared at an elevation angle of about 24.5 degrees.

The analysis of the obtained time series of azimuth and elevation angles results in power density spectra (P_A and P_E) and associated confidence limits which represent the observed random angle variations, see also Figs. 12 and 13. The effect of manual chart reading errors on the observed PDS was also studied. It was shown to consist of a steep increase in the PDS at the high frequency end. The effect of thermal receiver noise on the observed random angle variations was kept at a negligible level.

The comparison of the predicted PDS of the random tropospheric angle errors for the Early Bird observations with the observed PDS leads to the conclusion that the observed random angle variations are indeed caused by the troposphere. In particular it is found that the PDS of the azimuth and elevation observations (P_A and P_E in Figs. 12 and 13), within their respective confidence limits (P_{A1} , P_{A2} ; P_{E1} , P_{E2}), lie almost exactly on the predicted *minimum* power density spectra ($P_{A,\,\min}$; $P_{E,\,\min}$) for random tropospheric angle errors.

The feasibility of acquiring additional data on tropospheric propagation effects, especially random angle errors, with the Andover horn antenna on geo-stationary satellites of the Early Bird type, therefore, was also demonstrated.

VI. ACKNOWLEDGMENTS

The author gratefully acknowledges the assistance by M. B. Allen, Jr. and W. A. Klute of Bell Laboratories, as well as that by T. F. Palmatier and his personnel of the AT&T Long Lines Department in Andover, Me. in the acquisition of the angle measurements. The manual digitizing of the analog strip chart records was performed with the help of Mrs. C. Unger. Valuable advice and encouragement for this publication were received from C. A. Armstrong, P. V. Dimock, and M. P. Wilson.

APPENDIX

Numerical Calculation of Predicted PDS

The *parameters* of the tracking situation during the Early Bird observations on May 7, 1965, which permit the prediction of the tropospheric angle PDS with the described model are:

transmission frequency $= f_t = 4137.86$ [MHz]
antenna diameter $= d = 67.7$ [ft] $= 20.6$ [m]
beamwidth $= \theta = 0.225$ [deg]
apparent elevation angle $= E_a \approx 24.5$ [deg]
azimuth angle $= A \approx 128.5$ [deg]
altitude of horn antenna $= h_1 = 900$ [ft] $= 274$ [m]
altitude of satellite $= h_2 \approx 22{,}200$ [st. mi.] $\approx 35{,}700$ [km]
slant-range $= R_{12} \approx 24{,}300$ [st. mi.] $\approx 39{,}100$ [km]
wind vector: $|\hat{w}| = 19$ [st. mi/hr]; $\delta = 0°$
surface refractivity $= N_s = 301$

With these parameters the *model functions* for this tracking situation are calculated as follows.

Breakfrequency of the angle scale function, (15):

$$f_1 = 2.43 \times 10^{-2} \text{ [Hz]}.$$

Angle scale function, (14):

$$S_\alpha = 20\,(f/\text{Hz})^2\,(1/\text{m}^2] \quad \text{for} \quad 0 \leqq f \leqq 2.43 \times 10^{-2} \text{ [Hz]}$$

$$S_\alpha = 1.18 \times 10^{-2}\,[1/\text{m}^2] \quad \text{for} \quad 2.43 \times 10^{-2} \text{ [Hz]} \leqq f \leqq \infty.$$

Breakfrequency for aperture smoothing, (17):

$$f_2 = 9.71 \times 10^{-2} \text{ [Hz]}.$$

Aperture smoothing function, (16):

$$\Phi_\alpha = 1 \qquad \text{for} \quad 0 \leqq f \leqq 9.71 \times 10^{-2} \text{ [Hz]}$$

$$\Phi_\alpha = 9.43 \times 10^{-3} \, (f/\text{Hz})^{-2} \quad \text{for} \quad 9.71 \times 10^{-2} \text{ [Hz]} \leqq f \leqq \infty.$$

Effective tropospheric path length, (19) and (20):

$$L = 8.02 \text{ [km]}.$$

Effective path length function, (18):

$$\Lambda = 0.534 \quad \text{for} \quad 0 \leqq f \leqq \infty.$$

Weather functions:

minimum: $W_{\min} = 1$ (by definition of P_m)

maximum: $W_{\max}$ as per (22).

Effective wind speed, azimuth, (30):

$$u_A = 14.9 \text{ [st. mi/hr]} = 6.7 \text{ [m/sec]}.$$

Effective wind speed, elevation, (33):

$$u_E = 4.9 \text{ [st. mi/hr]} = 2.2 \text{ [m/sec]}.$$

Effective wind function for transformation of the power density, azimuth, (26):

$$U_{PA} = 0.149^{\gamma+1}.$$

Effective wind function for transformation of the frequency regions, azimuth, (27):

$$U_{fA} = 6.7.$$

Effective wind function for transformation of the power density, elevation, (26):

$$U_{PE} = 0.455^{\gamma+1}.$$

Effective wind function for transformation of the frequency regions, elevation, (27):

$$U_{fE} = 2.2.$$

The operation with these model functions on the range model PDS $P_m\{f\}$ results in the following four *predicted PDS of tropospheric random angle errors.*

Minimum PDS in azimuth:

$$P_{A,\min} = \begin{cases} 7.57 \times 10^{+16}\,(f/\mathrm{Hz})^{+4}\ [\mathrm{rad}^2/\mathrm{Hz}] \\ \qquad \text{for} \quad 0 \leqq f \leqq 1.68 \times 10^{-7}\ [\mathrm{Hz}] \\ 3.55 \times 10^{-4}\,(f/\mathrm{Hz})^{+1}\ [\mathrm{rad}^2/\mathrm{Hz}] \\ \qquad \text{for} \quad 1.68 \times 10^{-7} \leqq f \leqq 6.70 \times 10^{-5}\ [\mathrm{Hz}] \\ 1.95 \times 10^{-10}\,(f/\mathrm{Hz})^{-0.5}\ [\mathrm{rad}^2/\mathrm{Hz}] \\ \qquad \text{for} \quad 6.70 \times 10^{-5} \leqq f \leqq 6.70 \times 10^{-3}\ [\mathrm{Hz}] \\ 1.60 \times 10^{-11}\,(f/\mathrm{Hz})^{-1}\ [\mathrm{rad}^2/\mathrm{Hz}] \\ \qquad \text{for} \quad 6.70 \times 10^{-3} \leqq f \leqq 1.63 \times 10^{-1}\ [\mathrm{Hz}] \\ 4.25 \times 10^{-13}\,(f/\mathrm{Hz})^{-3}\ [\mathrm{rad}^2/\mathrm{Hz}] \\ \qquad \text{for} \quad 1.63 \times 10^{-1} \leqq f \leqq 6.51 \times 10^{-1}\ [\mathrm{Hz}] \\ 1.81 \times 10^{-13}\,(\mathrm{f}/\mathrm{Hz})^{-5}\ [\mathrm{rad}^2/\mathrm{Hz}] \\ \qquad \text{for} \quad 6.51 \times 10^{-1} \leqq f \leqq 6.70 \times 10^{+2}\ [\mathrm{Hz}] \\ 5.47 \times 10^{-5}\,(f/\mathrm{Hz})^{-8}\ [\mathrm{rad}^2/\mathrm{Hz}] \\ \qquad \text{for} \quad 6.70 \times 10^{+2} \leqq f \leqq \infty\ [\mathrm{Hz}] \end{cases}$$

Maximum PDS in azimuth:

$$P_{A,\max} = \begin{cases} 4.54 \times 10^{+17}\,(f/\mathrm{Hz})^{+4}\ [\mathrm{rad}^2/\mathrm{Hz}] \\ \qquad \text{for} \quad 0 \leqq f \leqq 1.68 \times 10^{-7}\ [\mathrm{Hz}] \\ 2.13 \times 10^{-3}\,(f/\mathrm{Hz})^{+1}\ [\mathrm{rad}^2/\mathrm{Hz}] \\ \qquad \text{for} \quad 1.68 \times 10^{-7} \leqq f \leqq 1.49 \times 10^{-4}\ [\mathrm{Hz}] \\ 3.90 \times 10^{-9}\,(f/\mathrm{Hz})^{-0.5}\ [\mathrm{rad}^2/\mathrm{Hz}] \\ \qquad \text{for} \quad 1.49 \times 10^{-4} \leqq f \leqq 1.63 \times 10^{-1}\ [\mathrm{Hz}] \\ 1.03 \times 10^{-10}\,(f/\mathrm{Hz})^{-2.5}\ [\mathrm{rad}^2/\mathrm{Hz}] \\ \qquad \text{for} \quad 1.63 \times 10^{-1} \leqq f \leqq 6.51 \times 10^{-1}\ [\mathrm{Hz}] \\ 4.38 \times 10^{-11}\,(f/\mathrm{Hz})^{-4.5}\ [\mathrm{rad}^2/\mathrm{Hz}] \\ \qquad \text{for} \quad 6.51 \times 10^{-1} \leqq f \leqq 6.70 \times 10^{-1}\ [\mathrm{Hz}] \\ 3.61 \times 10^{-11}\,(f/\mathrm{Hz})^{-5}\ [\mathrm{rad}^2/\mathrm{Hz}] \\ \qquad \text{for} \quad 6.70 \times 10^{-1} \leqq f \leqq 6.70 \times 10^{+2}\ [\mathrm{Hz}] \\ 1.09 \times 10^{-2}\,(f/\mathrm{Hz})^{-8}\ [\mathrm{rad}^2/\mathrm{Hz}] \\ \qquad \text{for} \quad 6.70 \times 10^{+2} \leqq f \leqq \infty\ [\mathrm{Hz}] \end{cases}$$

Minimum PDS in elevation:

$$P_{E,\min} = \begin{cases} 2.01 \times 10^{+19}\ (f/\mathrm{Hz})^{+4}\ [\mathrm{rad}^2/\mathrm{Hz}] \\ \qquad \text{for} \quad 0 \leqq f \leqq 5.50 \times 10^{-8}\ [\mathrm{Hz}] \\ 3.31 \times 10^{-3}\ (f/\mathrm{Hz})^{+1}\ [\mathrm{rad}^2/\mathrm{Hz}] \\ \qquad \text{for} \quad 5.50 \times 10^{-8} \leqq f \leqq 2.20 \times 10^{-5}\ [\mathrm{Hz}] \\ 3.41 \times 10^{-10}\ (f/\mathrm{Hz})^{-0.5}\ [\mathrm{rad}^2/\mathrm{Hz}] \\ \qquad \text{for} \quad 2.20 \times 10^{-5} \leqq f \leqq 2.20 \times 10^{-3}\ [\mathrm{Hz}] \\ 1.60 \times 10^{-11}\ (f/\mathrm{Hz})^{-1}\ [\mathrm{rad}^2/\mathrm{Hz}] \\ \qquad \text{for} \quad 2.20 \times 10^{-3} \leqq f \leqq 5.35 \times 10^{-2}\ [\mathrm{Hz}] \\ 4.57 \times 10^{-14}\ (f/\mathrm{Hz})^{-3}\ [\mathrm{rad}^2/\mathrm{Hz}] \\ \qquad \text{for} \quad 5.35 \times 10^{-2} \leqq f \leqq 2.14 \times 10^{-1}\ [\mathrm{Hz}] \\ 2.09 \times 10^{-15}\ (f/\mathrm{Hz})^{-5}\ [\mathrm{rad}^2/\mathrm{Hz}] \\ \qquad \text{for} \quad 2.14 \times 10^{-1} \leqq f \leqq 2.20 \times 10^{+2}\ [\mathrm{Hz}] \\ 2.22 \times 10^{-8}\ (f/\mathrm{Hz})^{-8}\ [\mathrm{rad}^2/\mathrm{Hz}] \\ \qquad \text{for} \quad 2.20 \times 10^{+2} \leqq f \leqq \infty\ [\mathrm{Hz}] \end{cases}$$

Maximum PDS in elevation:

$$P_{E,\max} = \begin{cases} 1.21 \times 10^{+20}\ (f/\mathrm{Hz})^{+4}\ [\mathrm{rad}^2/\mathrm{Hz}] \\ \qquad \text{for} \quad 0 \leqq f \leqq 5.50 \times 10^{-8}\ [\mathrm{Hz}] \\ 1.99 \times 10^{-2}\ (f/\mathrm{Hz})^{+1}\ [\mathrm{rad}^2/\mathrm{Hz}] \\ \qquad \text{for} \quad 5.50 \times 10^{-8} \leqq f \leqq 4.91 \times 10^{-5}\ [\mathrm{Hz}] \\ 6.81 \times 10^{-9}\ (f/\mathrm{Hz})^{-0.5}\ [\mathrm{rad}^2/\mathrm{Hz}] \\ \qquad \text{for} \quad 4.91 \times 10^{-5} \leqq f \leqq 5.35 \times 10^{-2}\ [\mathrm{Hz}] \\ 1.95 \times 10^{-11}\ (f/\mathrm{Hz})^{-2.5}\ [\mathrm{rad}^2/\mathrm{Hz}] \\ \qquad \text{for} \quad 5.35 \times 10^{-2} \leqq f \leqq 2.14 \times 10^{-1}\ [\mathrm{Hz}] \\ 8.91 \times 10^{-13}\ (f/\mathrm{Hz})^{-4.5}\ [\mathrm{rad}^2/\mathrm{Hz}] \\ \qquad \text{for} \quad 2.14 \times 10^{-1} \leqq f \leqq 2.20 \times 10^{-1}\ [\mathrm{Hz}] \\ 4.17 \times 10^{-13}\ (f/\mathrm{Hz})^{-5}\ [\mathrm{rad}^2/\mathrm{Hz}] \\ \qquad \text{for} \quad 2.20 \times 10^{-1} \leqq f \leqq 2.20 \times 10^{+2}\ [\mathrm{Hz}] \\ 4.43 \times 10^{-6}\ (f/\mathrm{Hz})^{-8}\ [\mathrm{rad}^2/\mathrm{Hz}] \\ \qquad \text{for} \quad 2.20 \times 10^{+2} \leqq f \leqq \infty\ [\mathrm{Hz}] \end{cases}$$

REFERENCES

1. Chernov, L. A., *Wave Propagation in a Random Medium*, McGraw-Hill Book Co., New York, 1960.
2. Tatarski, V. I., *Wave Propagation in a Turbulent Medium*, McGraw-Hill Book Co., New York, 1961.
3. Bode, H. W. and Shannon, C. E., A Simplified Derivation of Linear Least Squares Smoothing and Prediction Theory, Proc. IRE, April, 1950, pp. 417–425.
   Darlington, S., Linear Least-Squares Smoothing and Prediction with Applications, B.S.T.J., *37*, September, 1958, pp. 1221–1294.
4. Thompson, M. C., Jr. and Janes, H. B., Measurements of Phase Stability Over a Low-Level Tropospheric Path, J. Res. NBS, *63D*, 1, July–August, 1959, pp. 54–51.
5. Thompson, M. C., Jr., Janes, H. B., and Kirkpatrick, A. W., An Analysis of Time Variations in Tropospheric Refractive Index and Apparent Radio Path Length, J. Geophys. Res., *65*, 1, January, 1960, pp. 193–201.
6. Norton, K. A., et al., An Experimental Study of Phase Variations in Line-of-Sight Microwave Transmissions, NBS Monograph 33, November 1, 1961.
7. Janes, H. B. and Thompson, M. C., Jr., An Experimental Study of Atmospheric Errors in Microwave Range and Range Difference Measurements, NBS Report 7908, June 25, 1963.
8. Bean, B. R. and Thayer, G. D., Models of the Atmospheric Radio Refractive Index, Proc. IRE, May, 1959, pp. 740–755.
9. Hines, J. N., Tingye Li, Turrin, R. H., The Electrical Characteristics of the Conical Horn-Reflector Antenna, B.S.T.J., *42*, July, 1963, pp. 1187.
10. Githens, J. A., Kelly, H. P., Lozier, J. C., and Lundstrom, A. A., Antenna Pointing System: Organization and Performance, B.S.T.J., *42*, July, 1963, pp. 1213.
11. Githens, J. A. and Peters, T. R., Digital Equipment for the Antenna Pointing System, B.S.T.J., *42*, July, 1963, pp. 1223.
12. Lozier, J. C., Norton, J. A., and Iwama, M., The Servo System for Antenna Positioning, B.S.T.J., *42*, July, 1963, pp. 1253.
13. Cook, J. S. and Lowell, R., The Autotrack System, B.S.T.J., *42*, July, 1963, pp. 1283.
14. Smith, D. H., Carlson, C. P., McCune, R. J., Elicker, R. E., and Sageman, R. E., Planning, Operation, and External Communications of the Andover Earth Station, B.S.T.J., *42*, July, 1963, pp. 1383.
15. Anders, J. V., Higgins, E. F., Jr., Murray, J. L., and Schaefer, F. J., Jr., The Precision Tracker, B.S.T.J., *42*, July, 1963, pp. 1330.
16. Early Bird, TRW Space Log, TRW Systems, Redondo Beach, California, Summer 1965, pp. 33, 34.
17. Blackman, R. B. and Tukey, J. W., *The Measurement of Power Spectra*, Dover Publications, Inc., New York, 1958.
18. Violette, A., personal communication.
19. Bennett, W. R., Spectra of Quantized Signals, B.S.T.J., *27*, July, 1948, pp. 446–472.
20. Kennedy, J. T. and Rosson, J. W., The Use of Solar Radio Emission for the Measurement of Radar Angle Errors, B.S.T.J., *41*, November, 1962, pp. 1799–1812.
21. Barton, D. K., *Radar System Analysis*, Prentice-Hall, Inc., Englewood Cliffs, N. J., 1965.